Peer review status:
This is a non-peer-reviewed preprint submitted to EarthArXiv.

Global Gravitational-Resonant Waves in the Arctic Basin: Visualizing Hidden Ocean Macrodynamics using 22-Year Passive Microwave Radiometry Data

Elena B. Sapershtein [1] *(super_e@mail.ru)
Evgeniy I. Makarov [1](john143_143@mail.ru)
Igor A. Sapershtein [1] (sapershteyn@mail.ru)

[1] Independent Researcher, St. Petersburg, Russia

* Corresponding author

Elena B. Sapershtein — ORCID: https://orcid.org/0009-0009-7928-9989

Global Gravitational-Resonant Waves in the Arctic Basin: Visualizing Hidden Ocean Macrodynamics using 22-Year Passive Microwave Radiometry Data

Elena B. Sapershtein [1] *, Evgeniy I. Makarov [1], Igor A. Sapershtein [1]

[1] Independent Researcher, St. Petersburg, Russia

* Corresponding author: super_e@mail.ru

Elena B. Sapershtein — ORCID: https://orcid.org/0009-0009-7928-9989

Abstract

The dynamics of the Arctic Ocean's sea ice cover are traditionally viewed through the lens of atmospheric forcing, ocean currents, and thermodynamic processes. In this paper, we propose a fundamentally new paradigm: the sea ice cover acts not as an elastic membrane transmitting mechanical stress, but as a passive two-dimensional indicator (analogous to Chladni figures) that visualizes a macroscopic network of gravitational standing waves in the hydrosphere. Using a 22-year archive (2002–2025) of AMSR-E/AMSR2 passive microwave sea ice concentration data, we developed a novel spatial analysis methodology based on the Radon transform to extract low-frequency kinematic structures from high-frequency radiometric fluctuations. Traditionally discarded as noise, >100% ice concentration anomalies were reinterpreted as volumetric compaction and thickening in convergence zones.

The analysis reveals the existence of five strictly stable transarctic wave axes (0°, 30°, 60°, 120°, 150°) rigidly anchored to the basin's bathymetry (e.g., the Lomonosov Ridge). Spectral and circular variance analyses demonstrate that the wavelengths are highly clustered, proving that the Arctic Basin operates as a closed hydrodynamic resonator. Tracking the spatial phase of these waves over two decades revealed a non-linear, sawtooth kinematic evolution. Cross-correlation with astronomical ephemerides demonstrated that abrupt phase shifts (structural breakdowns of the ice cover) are strictly synchronized with syzygies (46.7% correlation), lunar perigee, and planetary alignments. Our findings challenge the wind-driven paradigm of large-scale sea ice

mechanics and offer a new geodynamic framework with profound implications for long-term meteorological and oceanographic forecasting.

Keywords

Arctic Basin, ocean macrodynamics, passive microwave radiometry, Radon transform, resonant standing waves, sea ice kinematics.

1. INTRODUCTION

The dynamics of the Arctic Ocean's sea ice cover are traditionally viewed through the lens of atmospheric forcing, ocean currents, and thermodynamic processes. Existing global satellite monitoring methods, such as radar and laser altimetry (CryoSat-2, ICESat-2), provide high accuracy in measuring ice thickness and sea level, but they suffer from a significant drawback—low temporal resolution (temporal aliasing). The need to average data over periods ranging from several weeks to a month smooths out high-frequency (diurnal and semidiurnal) gravitational-tidal processes. At the same time, classic works [Maximov, 1970] convincingly demonstrated that the long-period wave dynamics of the hydrosphere are largely determined not so much by atmospheric forcing, but by global geophysical and astronomical forces. On the other hand, contact measurements using drifting buoys and tiltmeters (e.g., the IABP program [Thorndike & Colony, 1982]) reliably record local tidal deformations and ice compressions, yet their point-based nature prevents the reconstruction of the macroscopic spatial geometry of wave processes across the entire basin. As a result, the global picture of the gravitationally-induced dynamics of the Arctic Ocean remains hidden.

In this paper, a fundamentally new approach to the interpretation of passive microwave radiometry data (AMSR-E / AMSR2) is proposed. Traditionally, algorithms calculating Sea Ice Concentration (SIC) interpret value fluctuations in highly concentrated (10/10) winter ice as

instrumental or atmospheric noise, often artificially capping the upper limit at 100%. We hypothesize that these brightness temperature fluctuations are a highly accurate signal reflecting changes in volumetric density, increased deformation, and local ice thickness in zones of macroscopic kinematic compression.

Relying on this postulate, we depart from the classic perception of the sea ice cover as a mechanical elastic membrane transmitting stresses over thousands of kilometers. Instead, the sea ice cover is viewed as a massive passive two-dimensional indicator (analogous to Chladni figures) that visualizes a grid of gravitational standing waves in the underlying hydrosphere. A key mechanism in the formation of the observed structures is the presence of colossal volumes of free frazil and sub-ice accumulations, historically noted in field observations by icecaptains and divers [Burke, 1940], but ignored in modern satellite models. This free ice, possessing a different density compared to seawater, acts as a hydrothermodynamic tracer [Nazirov, 1982], instantly redistributing and accumulating at the nodes of the basin's resonances, forming linear zones of maximum ice mass concentration visible from the satellite.

To extract these hidden structures from the seemingly chaotic sea ice cover, a global spatial analysis method based on the Radon Transform was applied for the first time. The analysis of daily satellite matrices over a 22-year period (2002–2025) allowed us not only to reveal the existence of discrete transarctic standing waves (resonant modes) but also to track their phase kinematics.

The objective of this study is to extract these hidden macrostructures and to statistically and physically prove their gravitational-resonant nature. The article shows that the detected wave modes possess a rigid geographical anchoring to the Arctic Ocean bathymetry, and the moments

of their structural reorganization (phase shifts) are synchronized with key orbital mechanics events: syzygies, lunar perigee passages, and planetary alignments.

2. DATA AND METHODS

2.1. Satellite Data

Daily global Sea Ice Concentration (SIC) matrices derived from passive microwave radiometry using the AMSR-E and AMSR2 satellite sensors (ASI algorithm, University of Bremen) [Spreen et al., 2008; Melsheimer & Spreen, 2019, 2020] were used as the primary data source. The spatial resolution of the source grids is 6.25 km. To exclude the influence of thermodynamic processes, the analysis was conducted exclusively for winter periods (November to June) over a 22-year interval.

2.2. Pre-processing and Trough Extraction

To extract low-frequency macrostructures from the noisy high-frequency field, spatial averaging (downsampling to ~50 km) was applied, followed by a cascade of median and Gaussian filtering. Contrast Limited Adaptive Histogram Equalization (CLAHE) was used to enhance weak gradients.

A critical step was the mathematical isolation of zones with anomalously high local ice concentration, physically corresponding to the troughs (convergence zones). The focus was shifted specifically to troughs, as they are considered areas of the primary gravitational response of the system. Based on threshold filtering, background values were zeroed out, retaining the gradient only within the axes of maximum kinematic compression.

2.3. Mathematical Detection of Wave Axes (Radon Transform)

The search for global linear structures was implemented using the Radon Transform [Chapman, 1981]. The integral equation for the intensity field $f(x, y)$ is given by Eq. (1):

$$R(\rho, \theta) = \iint_{-\infty}^{\infty} f(x, y)\delta(\rho - x\cos\theta - y\sin\theta)dxdy \quad (1)$$

To eliminate false edge effects from the complex coastal geometry, the algorithm employed chord-length profile normalization within the ocean mask and edge apodization windowing. The orthogonals to the angles of the maxima on the sinogram determined the geographical azimuths of the linear wave fronts (see Figure 1).

2.4. Spectral Estimation and Spatial Phase Tracking

For each extracted direction, a one-dimensional profile was extracted, to which a Fast Fourier Transform (FFT) was applied to determine the macroscopic wavelength λ (from 700 to 4000 km).

Then, a two-dimensional directional bandpass filter was applied in the Fourier space. The inverse transform reconstructed an ideal mathematical cosine wave. The final parameter for daily monitoring was the spatial phase Φ(t) (the shift of the wave grid relative to the pole), which allowed us to localize the moments of structural reorganizations (phase breakdowns/shifts).

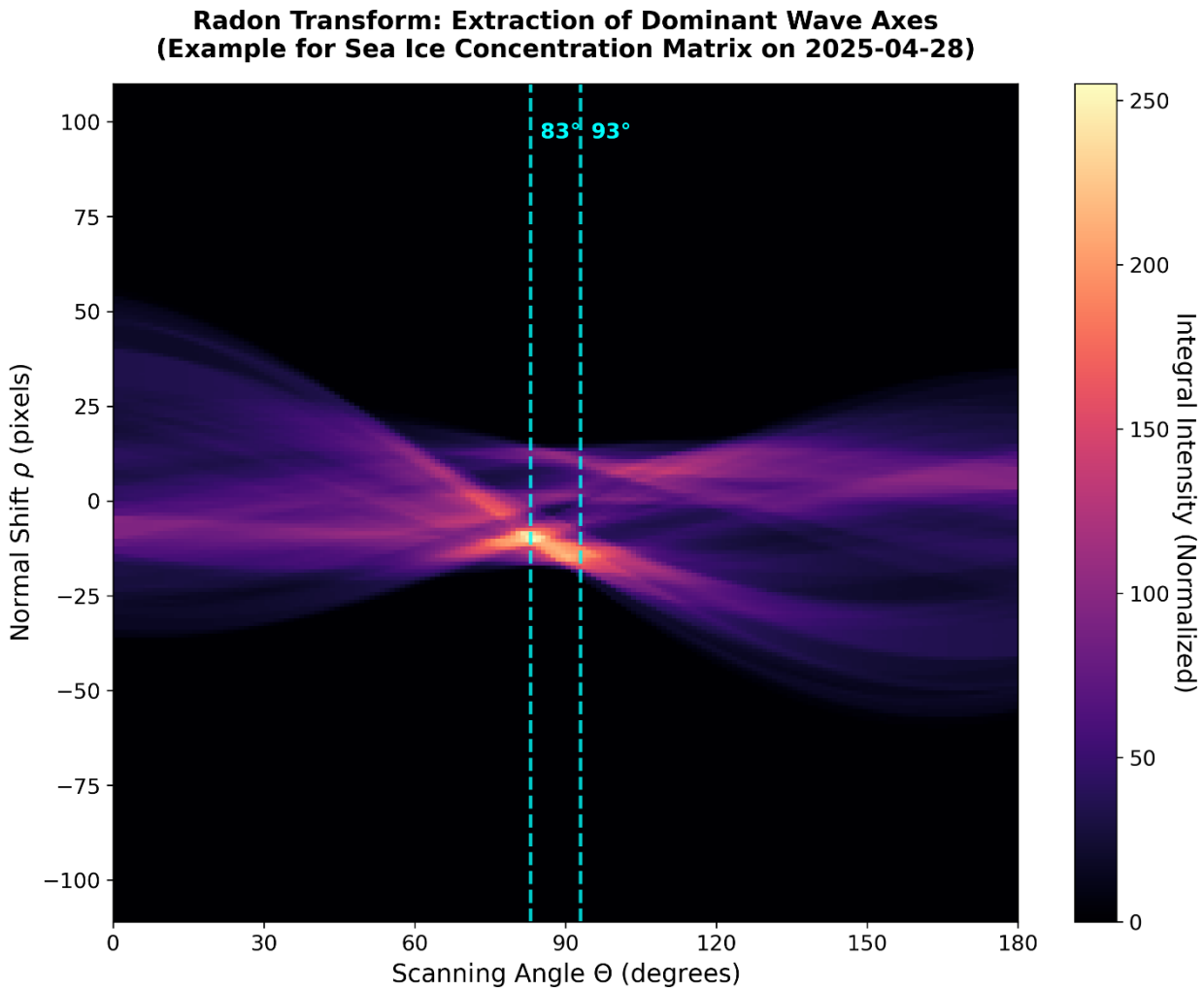

Figure 1: Example of the Radon Transform. Maxima of integral intensity indicate scanning angles Θ corresponding to the dominant axes of kinematic compression in the sea ice cover. (Note: The Python script for this data visualization was generated with the assistance of Cursor AI).

3. RESULTS

3.1. Global Resonant Axes

Applying the Radon Transform revealed a stable spatial quantization of wave processes. Unlike chaotic wind-driven drift, macroscopic troughs form along five strictly defined transarctic axes: 0°, 30°, 60°, 120°, and 150°.

An analysis of the Circular Variance of the spatial phase Φ showed their exceptional stability. For fundamental macro-modes (wavelengths 1300–3500 km), the variance was only 0.10–0.20,

proving their rigid anchoring to the basin's coordinate grid. Conversely, short-period modes (700–1000 km) exhibited high variance. Since only standing waves whose geometry is a multiple of the physical boundaries of the basin can exist, these higher harmonics (overtones) resonate between closer local boundaries or relief elements, rather than between the fundamental boundaries of the entire Arctic Ocean.

3.2. Clustering of Wave Parameters

A crucial result confirming the resonant nature of the hydrosphere is the clustering of wavelengths. Spectral analysis of data over 22 years established that wavelengths are not uniformly distributed but are clustered around discrete values corresponding to specific geographical azimuths. Each direction (e.g., 120°) corresponds to a strictly defined set of permitted wavelengths (a fundamental mode and its harmonics). This mathematically proves that the Arctic Basin operates as a giant closed resonator, where only standing waves with geometry proportional to the physical boundaries of the basin can exist (see Figure 2). It is worth noting that the phenomenon of large-scale resonant effects in the stratified liquids of the Arctic Basin, leading to the emergence of anomalously strong "extra-currents", was theoretically predicted earlier [Nikiforov, 2004]. Our satellite analysis visually and statistically confirms the presence of this global resonant system directly in the sea ice cover for the first time.

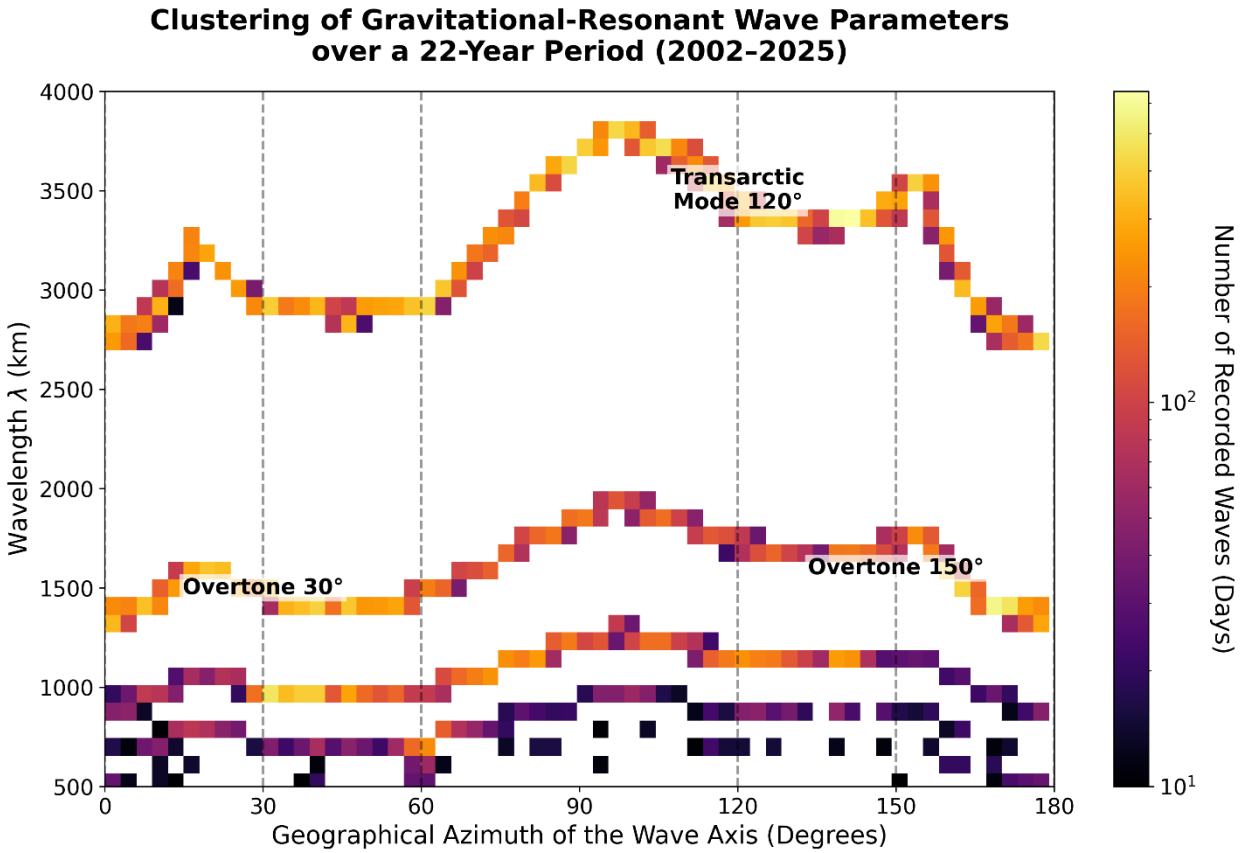

Figure 2: 2D Heatmap of wavelength distribution depending on geographic azimuth over 22 years. Distinct discrete clusters prove the quantization of hydrosphere resonances in the Arctic Basin. (Note: The Python script for this data visualization was generated with the assistance of Cursor AI).

3.3. Geographical Anchoring to Bathymetry

Overlaying the resonance grid onto the Arctic Ocean bathymetric map revealed a direct correspondence between standing wave nodes and bottom topography. The transarctic 120° mode (wavelength ~3500 km) runs parallel to the Lomonosov Ridge. The 30° and 60° modes form an orthogonal antinode system over the deep Amundsen Basin, while one of the 30° axes points towards the Fram Strait. These coincidences confirm that submarine ridge geometry acts as a physical resonator dictating the position of standing waves (see Figure 3).

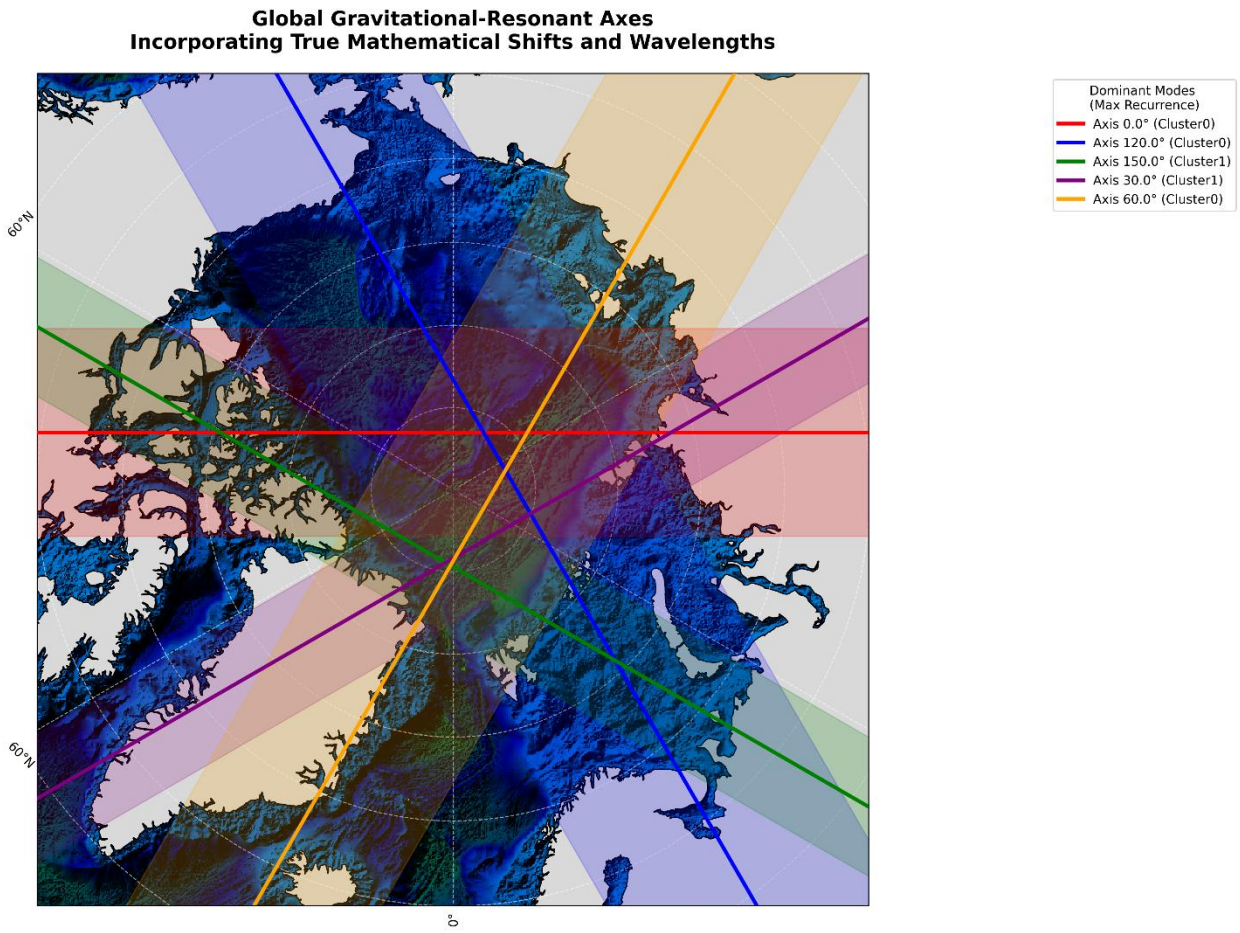

Figure 3: Five main transarctic gravitational-resonant axes of ice compression. The axes are strictly anchored to bottom topography (background: IBCAO bathymetry). (Note: The Python script for this data visualization was generated with the assistance of Cursor AI).

3.4. Temporal Dynamics and Phase Kinematics

Analysis of phase time series revealed a sawtooth evolutionary profile. During periods of stress accumulation, the trough axis drifts smoothly. Upon reaching a threshold, an instantaneous (within 1-2 days) phase breakdown occurs—a stepwise shift of the grid by hundreds of kilometers. This process is accompanied by macroscopic compressions, intense dynamic deformations of the ice cover, and global rupturing of its continuity in tension zones.

4. LINK TO ORBITAL MECHANICS

4.1. Correlation of Phase Shifts with Astronomical Events

A cross-correlation analysis of phase breakdown moments with ephemerides over 22 years showed that out of 366 winter syzygies, 46.7% were accompanied by a global phase breakdown of at least one resonant mode (±2 days). The fact that 53.3% of syzygies were "blanks" points to the threshold nature of the interaction: a breakdown occurs only upon reaching a critical level of kinematic stress (see Figure 4).

Figure 4: Synchronization of ice kinematics with orbital mechanics using the 120° mode. (A) Sawtooth evolution of spatial phase; (B) Phase shift velocity highlighting breakdown moments (anomalies); (C) Coincidence of phase breakdowns with syzygies (full moons and new moons). (Note: The Python script for this data visualization was generated with the assistance of Cursor AI).

4.2. Role of Additional Orbital Triggers

The most powerful phase breakdowns are recorded under a superposition of factors: the coincidence of a syzygy with the Moon's perigee passage and extreme values of lunar declination. Planetary alignments (Planetary Alignment Index) also exert significant influence. The alignment of the gravity vectors of giant planets (Jupiter and Saturn), as well as Venus, frequently acts as the final trigger for stress release.

4.3. Asynchrony and Cascading Stress Release

The percentage of simultaneous breakdowns (±1 day) for different axes within the same wavelength cluster does not exceed 12%. Harmonics on the same axis also break down asynchronously. This proves that the clusters represent independent physical resonances. The forcing acts selectively, ensuring cascading stress release and preventing the simultaneous total destruction of ice throughout the basin.

5. DISCUSSION

5.1. Primacy of Troughs and Shift in the Earth's Center of Mass

Traditional oceanography views the tidal crest as the primary response to the gravity of celestial bodies. However, building on V.I. Danilov's hypothesis [Danilov, 2023] regarding the primacy of troughs, our macroscopic satellite analysis definitively confirms this concept on a global level. Gravitational influence shifts the Earth's barycenter within the mantle. This locally increases gravity, forcing water and ice to rush into convergence zones (gravitational "pits"). Thus, the trough acts as the primary reaction of the system, while the crest is a secondary compensatory response. Focusing the algorithm specifically on the troughs was key to isolating stable axes.

5.2. The Observer Principle and the Uniqueness of the Sea Ice Cover as a Sensor

The historical invisibility of these waves to contact measurements (buoys, tiltmeters) is explained by the principle of relativity: being inside the water, the sensor only records the local orbital drift of particles. Unlike buoys, the continuous sea ice cover acts as a global integral strain gauge. Satellite observation from an external frame of reference visualizes the spatial gradients of macroscopic deformation, turning the sea ice cover into an "oscilloscope screen" for the gravitational field.

5.3. Concentration vs. Volumetric Density: Terminology Revision

An important consequence of the proposed model is the revision of passive microwave radiometry data interpretation. In the official WMO nomenclature, concentration is defined as the 2D ratio of ice area to water area. However, in the central Arctic in winter, the coverage area is always close to 100%. Radiometric fluctuations (>100%), traditionally discarded as noise, de facto reflect changes in **volumetric concentration** and local **increases in ice thickness**. In standing wave nodes, compression leads to floe overriding, brine expulsion, and sub-ice accumulation, drastically altering radiometric emissivity. The AMSR signal is a physically robust indicator of kinematic stress.

5.4. Co-evolution of Lithosphere and Hydrosphere

It is intriguing to note that the directions of the gravitational mode fronts we identified strikingly align with the strike of major coastlines (e.g., axes along the coasts of Kamchatka and Eastern Siberia, Alaska and Canada, as well as the single line of the Severnaya Zemlya, Franz Josef Land, and Svalbard archipelagos). This allows us to put forward the bold hypothesis that the shapes of the lithosphere (coasts, submarine and surface ridges) and the wave modes of the hydrosphere do not simply coincide randomly, but historically co-evolved under the influence of a single planetary grid of gravitational standing waves.

6. CONCLUSION

Applying the Radon Transform to a 22-year archive of AMSR-E/AMSR2 data has proven that the Arctic sea ice cover functions as a global indicator of gravitational-resonant standing waves in the hydrosphere. The isolation of stable transarctic axes (0°, 30°, 60°, 120°, 150°) and their strict synchronization with the orbital mechanics of celestial bodies irrefutably confirm this paradigm.

The quality and value of microwave satellite data (AMSR) deserve special mention. Despite regional criticism of interpretation algorithms during melt periods, it is precisely these data, through their integral microwave response, that allowed us to "see" macrostructures for the first time and correctly reflect global geodynamic trends.

The proposed gravitational-resonant model opens new horizons not only in ice geophysics but across most Earth sciences. The traditional approach, where point measurements are interpolated via closed isolines, can be significantly improved. If we assume that the distribution of physical characteristics in the ocean (acoustic layers, salinity and temperature fronts) and the atmosphere (cyclone and anticyclone paths) is also governed by the geometry of gravitational standing waves, interpreting these fields through a wave grid will provide fundamentally new prerequisites for qualitative long-term forecasting.

Funding

This research did not receive any specific grant from funding agencies in the public, commercial, or not-for-profit sectors.

Declaration of generative AI and AI-assisted technologies in the manuscript preparation process

During the preparation of this work the author(s) used Cursor AI assistant in order to translate the text to English, correct grammar, and assist with the generation of Python scripts for data visualization. After using this tool/service, the author(s) reviewed and edited the content as needed and take(s) full responsibility for the content of the published article.

Data Availability Statement

The sea ice concentration data (AMSR-E and AMSR2, ASI algorithm) are available from the PANGAEA repository (Melsheimer and Spreen, 2019, 2020). The IBCAO bathymetry data are available from the GEBCO portal. Processed spatial phase statistics and algorithms are available from the authors upon request.

References

Burke, A. (1940). Sea Ice. Leningrad-Moscow: Glavsevmorput, 96 pp. (in Russian).

Chapman, C. H. (1981). Generalized Radon transforms and slant stacks. *Geophysical Journal International*, 66(2), 445-453. https://doi.org/10.1093/gji/66.2.445

Danilov, V.I. (2023). The New View at the Physics of the Planet Earth. *Global Journal of Science Frontier Research: A Physics and Space Science*, 23(1), 41-60. https://portalnp.snauka.ru/author/danvlad

Maximov, I. V. (1970). Geophysical Forces and Waters of the Ocean. Leningrad: Gidrometeoizdat, 447 pp. (in Russian).

Melsheimer, C., & Spreen, G. (2019). AMSR2 ASI sea ice concentration data, Arctic, version 5.4 [Data set]. PANGAEA. https://doi.org/10.1594/PANGAEA.898399

Melsheimer, C., & Spreen, G. (2020). AMSR-E ASI sea ice concentration data, Arctic, version 5.4 [Data set]. PANGAEA. https://doi.org/10.1594/PANGAEA.919777

Nazirov, M. (1982). Ice and suspensions as hydro-thermodynamic tracers from multispectral space survey data. Leningrad: Gidrometeoizdat, 165 pp. (in Russian).

Nikiforov, E. G. (2004). The phenomenon of extra-currents in the Arctic Basin and marginal Arctic seas (resonances in stratified liquids). St. Petersburg: AARI Rotaprint. (in Russian).

Spreen, G., Kaleschke, L., & Heygster, G. (2008). Sea ice remote sensing using AMSR-E 89-GHz channels. *Journal of Geophysical Research: Oceans*, 113(C2). https://doi.org/10.1029/2005JC003384

Thorndike, A. S., & Colony, R. (1982). Sea ice motion in response to geostrophic winds. *Journal of Geophysical Research: Oceans*, 87(C8), 5845-5852. https://doi.org/10.1029/JC087iC08p05845